Proceedings World Geothermal Congress 2020+1
Reykjavik, Iceland, April - October 2021

Temporal Evolution of Faults in the Southern German Molasse Basin: A Case Study of the Wolftratshausen Geothermal Prospect, Germany

Vladimir Shipilin[1,2], David C. Tanner[1], Hartwig von Hartmann[1], Inga Moeck[1,2]

[1]Leibniz Institute for Applied Geophysics, Stilleweg 2, D-30655 Hannover

[2] University of Göttingen, Goldschmidtstr. 3, D-37077 Göttingen

E-mail: vladimir.shipilin@leibniz-liag.de

Keywords: German Molasse Basin, Upper Jurassic carbonate platform, Play Type, foreland basin, fault kinematics, fault controlled reservoirs, decoupled deformation, geothermal exploration, seismic attributes.

ABSTRACT

Recently, foreland basins have become prime targets to host geothermal resources because of the existence of deep aquifers. Understanding of tectonic evolution and fault kinematics is crucial to evaluate the potential for geothermal energy production. Based on a 3D seismic survey, acquired 30 km south of Munich, we analyse fault patterns within the Upper Jurassic carbonate reservoir and its Molasse overburden within the geothermal prospect of Wolfratshausen, in the southern German Molasse Basin. To determine the temporal activity of the interpreted faults, we built a 3D geological model, from which we derived juxtaposition diagrams of the faulted strata and thickness maps of seismic horizons. We show that the strata at Wolfratshausen underwent different deformation phases; extension in the pre- and early-orogenic stages of basin formation and contraction in the Middle Miocene. Furthermore, the deformation style at this part of the basin is characterised by decoupled faulting. The identified structures, their temporal activity, and deformation style indicate active stress regime and thus provide an insight into the hydraulic transmissivity of the fault zones for geothermal exploration.

1. INTRODUCTION

In the last decade, there has been an increasing interest in foreland basins to host geothermal resources because of the existence of deep aquifers (e.g. Schulz et al., 2004; Weides and Majorowicz, 2014). As generally stated by Moeck (2014) for the orogenic belt/foreland play type, the major controls on permeability structure of the reservoir are lithology, facies, and fault networks. Hence, ideal targets of geothermal wells are extensively fractured massive carbonate facies that possessed high initial porosity. However, with increasing depth of the geothermal reservoir towards the orogenic belt, compaction decreases initial porosity and, as a result, faulting becomes the primary factor governing heat transport (Moeck, 2014).

Faults can act either as hydraulic conduits or as barriers to fluid flow, depending on their position in the current stress field and their kinematic history. Faults with high slip and dilation tendency, i.e. optimally oriented for failure in the present-day stress tensor, exhibit enhanced permeability and are therefore considered favourable to channel fluids, whereas compressional faults tend to be sealed (Anderson and Fairley, 2008; Sheridan and Hickman, 2004; Moeck et al., 2015, Budach et al., 2017). Kinematic evolution of faults is another essential knowledge that is required to infer fault conductivity. Faults that experienced episodic reactivation are less prone to be healed by secondary mineralisation processes (Moeck et al., 2015, Budach et al., 2017). Furthermore, analysis of geometric patterns and style of faulting is also valuable for the assessment of fault zone permeability. Intersection zones of crossing conjugate faults, as well as regions of segment linkage on individual faults are reported to be sites of enhanced permeability due to increased fracture density (Wilkins and Gross, 2002; Ferrill et al., 2009). Therefore, understanding of tectonic evolution and fault kinematics is crucial to evaluate potential geothermal reservoirs that lie at the required depths during the pre-drilling exploration stage.

Our working area is within the southernmost part of the German Molasse Basin (Fig. 1) — a typical foreland system. A number of basin-scale structural studies were carried out in the 80s and 90s, based on a large amount of 2D seismic data acquired over decades of hydrocarbon exploration (e.g. Bachmann et al., 1982; Bachmann et al., 1987; Müller et al., 1998; Bachmann and Müller, 1992). However, until recently there have been only a few detailed structural studies in relatively weakly-deformed parts of the foreland basin. Only with the emergence of geothermal exploration in the recent years and the consequent acquisition of 3D seismic data, have such studies become possible (e.g. Lüschen et al., 2011; von Hartmann et al., 2016; Budach et al., 2017).

In the present work, we focus on an in-depth analysis of deformation structures within the geothermal prospect of Wolfratshausen. Our aim is to understand the structure and tectonic evolution of an area proximal to the Alpine deformation front optimize geothermal exploration. Using a 3D seismic survey, we analyse fault patterns within the Upper Jurassic carbonate reservoir and its Molasse overburden. In particular, analysing juxtaposition diagrams (Allan, 1989) and thickness maps, we establish the relationship between sedimentation and faulting, as well as the temporal activity of faults. Based on the results of seismic interpretation and structural analysis, we discuss the permeability of the delineated fault zones looking at three main observations: (i) orientation of the faults within the present-day stress field, (ii) their kinematic history, and (iii) zones of possible fault linkage and interaction.

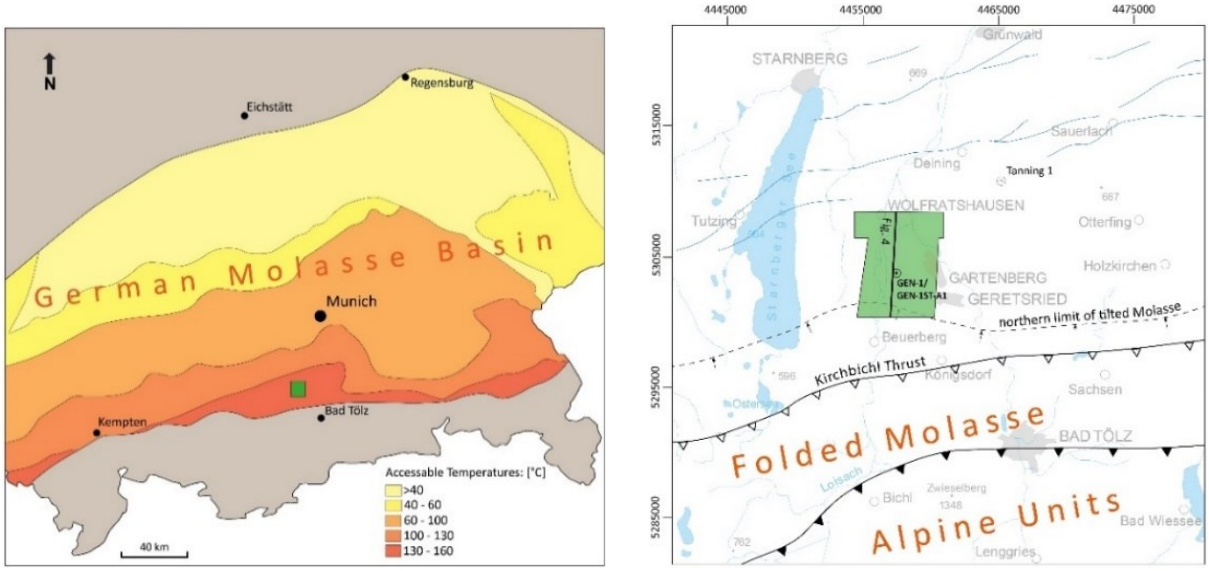

Figure 1: Location maps. *Left*: outline of the German Molasse Basin with geothermal areas (www.geotis.de), *right*: location of the Geretsried 3D seismic survey within the Wolfratshausen prospect. Black line marks profile within the survey area in Fig. 4, blue lines are major normal faults.

2. GEOLOGICAL SETTING

The German Molasse Basin is part of the North Alpine Foreland Basin that evolved on the subducting European margin, in front of the Alps, since the Late Eocene (Lemcke, 1973; Bachmann et al., 1982). The Cenozoic deposits of the foreland basin unconformably overlie the peneplained Mesozoic sedimentary basement and locally, Permo-Carboniferous clastic sediments and crystalline rocks (Lemcke, 1988; Sissingh, 1997).

From Jurassic to mid Cretaceous times, the pre-Molasse region evolved as an extensional passive margin (Frisch, 1979; Ziegler, 1990; Pfiffner, 1992). Submergence of the southern European shelf by the Tethys Ocean in the Late Jurassic led to the deposition of a gently-dipping Upper Jurassic carbonate platform (Meyer and Schmidt-Kaler, 1990). At the present, it serves as the main aquifer for geothermal energy production in the Molasse Basin. In the study area, the carbonate platform is overlain by thin, lithologically heterogeneous Cretaceous sediments (Fig. 2; Bachmann et al., 1987).

After a profound hiatus in sedimentation caused by the Late Cretaceous contractional event, deposition resumed in the Late Eocene (Ziegler 1995). It marks the inception of the foreland basin in response to the Euro-Adriatic collision (Frisch, 1979; Allen et al., 1991; Ziegler 1995). Loading and consequent flexure of the European foreland plate created a wedge-shaped basin fill (Allen et al., 1991). Flexural subsidence was accompanied by the formation of longitudinal (i.e. foredeep-parallel) normal faults, which show successively younger syn-sedimentary activity toward the north (Bachmann et al., 1982; Bachmann and Müller, 1992).

The Cenozoic Molasse cover was deposited in the course of two major transgressive-regressive cycles and can be subdivided into, from base to top; the Lower Marine Molasse (UMM), the Lower Freshwater Molasse (USM), the Upper Marine Molasse (OMM), and the Upper Freshwater Molasse (OSM) (Eisbacher, 1974; Fig. 2). The lowermost UMM consists of a transgressive sequence that ranges from shallow-marine sandstones and carbonates, to deep-water condensed shales and marls (Lemcke, 1988; Sissingh, 1997). This sequence passes upward into thick Rupelian clayey marls that were deposited during a sea-level standstill (Zweigel et al., 1998). Transition from UMM to USM is marked by the accumulation of regressive, shallow-marine to coastal Baustein Beds (Diem, 1986). These are overlain by fluvial Chattian and Aquitanian Sands.

Despite decreasing subsidence in the Burdigalian, the second transgressive-regressive cycle began with transgression of OMM clay marls over the Aquitanian-Burdigalian erosional unconformity (Lemcke, 1988; Zweigel et al., 1998). By the beginning of Langhian, terrestrial conditions prevailed across the entire GMB, as OSM was deposited (Lemcke, 1988). From c. 8.5 Ma onwards, the GMB experienced isostatically-induced uplift and erosion (Lemcke, 1974). Our study area is within a weakly-deformed part of the basin, referred to as Foreland Molasse, immediately north of the frontal thrust of the Subalpine Molasse. The Subalpine (Folded) Molasse was formed by thrusting and incorporation of the proximal foreland basin sediments into the Alpine front (Bachmann et al., 1987; Reinecker et al., 2010).

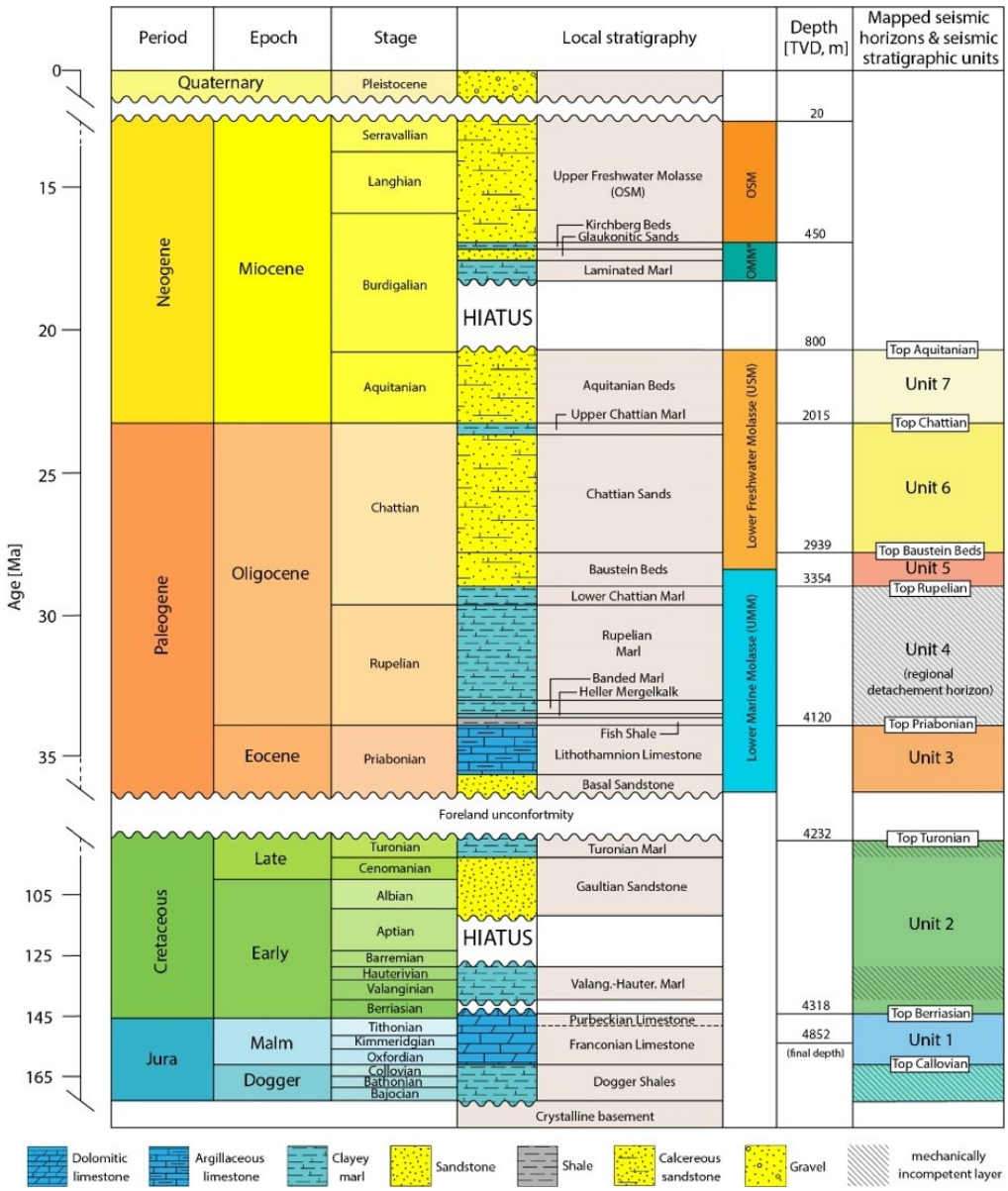

Figure 2: Detailed stratigraphy of the analysed area.

3. DATA AND METHODOLOGY

3.1 Database

The main database for this investigation is a Kirchoff pre-stack, depth-migrated, 3D seismic-reflection survey. It was acquired in 2010 for geothermal exploration and covers an area of c. 40 km^2 in the southern part of the German Molasse Basin (Fig. 1). The seismic volume has a record length of 5000 ms two-way travel time (TWT) with a 36-fold bin size of 25 m by 25 m. It is displayed with SEG standard polarity. The vertical stratigraphic resolution ranges from c. 20 m within the Cenozoic Molasse sediments to c. 55 m at the base of the carbonate platform, based on a dominant frequency range of 25–45 Hz and interval velocity range of 3500–5700 ms^{-1}.

The seismic reflection data are supplemented by vertical seismic profile and formation top data from the GEN-1 borehole (Fig. 2). We used time-to-depth picks obtained from the vertical seismic profiling to calibrate the interval migration velocities. The resultant velocity model was used for time-to-depth conversion, which was required for subsequent quantitative fault analysis in depth domain.

3.2 Methodology

The 3D seismic data cube was interpreted in the time domain using Schlumberger Petrel® seismic interpretation software. With a help of the vertical seismic profile the key seismic-stratigraphic horizons were tied to the well stratigraphy. This provided age constraints for six seismic horizons, which were mapped with a high degree of confidence across the dataset, from the top of the Purbeckian facies, which corresponds to the top Berriasian, up to the highest seismically recognizable horizon — the top Aquitanian (Fig.). In contrast, the base of the carbonate platform (top Callovian) was interpreted with a low degree of confidence due to poor vertical resolution and the absence of well control. We picked a low-frequency positive-phase reflector that is considered to be the base carbonate platform, given the 600–650 m thickness of the latter, which is reported for the southern part of the GMB (Lemcke, 1988).

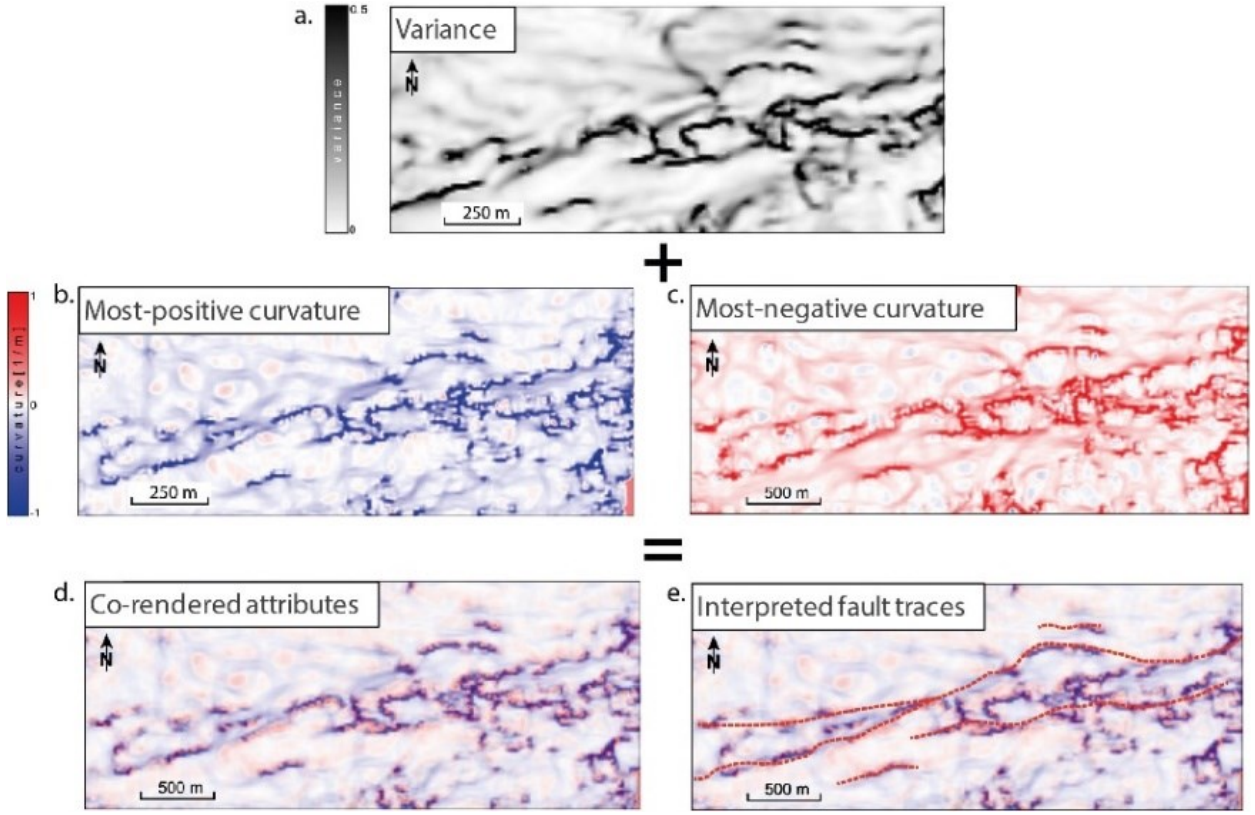

Figure 3: Time slice showing different attributes in different attribute display: (a) variance; (b) most-positive curvature; (c) most-negative curvature; (d) multiattribute display; (e) interpreted fault traces. Location of the horizontal slice in depth is shown in Figure 4.

In order to map fault patterns accurately within the seismic volume, we first applied data conditioning to the migrated seismic data by implementing a fault enhancement filter. This filter suppresses random noise and enhances amplitudes at fault locations, resulting in pronounced fault edges in the seismic reflection volume (Fig. 3a). Discontinuity anomalies in variance attribute volume, which are conventionally used to trace faults, become sharper, highlighting faults that have a discrete offset. In the relatively weakly-deformed Foreland Molasse, the majority of faults have a small offset of a few tens of metres (Bachmann et al., 1982). At tips of the faults, displacement may fall below the limits of seismic resolution and give rise to flexural deflection of reflections instead of a discrete offset. The flexural deformation does not appear in the variance volume; instead, it is detected by the curvature attribute. In order to map the full extent of the faults, we produced most-positive curvature and most-negative curvature attribute volumes and co-rendered them with variance into one multiattribute volume (e.g., Marfurt, 2015) (Fig.3e).

Consequently, the faults were traced on time-slices in multi-attribute display at arbitrary intervals and then were mapped on vertical sections in reflectivity display. The vertical sections were preferentially oriented perpendicular to the strike of the faults with a line spacing of 75–100 m.

After depth conversion, the interpreted stratigraphic horizons and faults were imported into SKUA-GOCAD® (Paradigm Ltd., 2017) for subsequent modelling. We firstly created horizon and fault surfaces and generated fault/horizon intersections to model fault displacement. We then produced juxtaposition diagrams by projecting fault displacement onto the modelled fault planes to determine timing of faulting and fault growth. Additionally, we created isochore maps to analyse syn- and post-sedimentary features.

3. RESULTS

The identified fault network within the study area is divided into two distinct fault arrays that are geometrically decoupled by the Rupelian claystone layer, and are thus referred to as the *lower fault array* (i.e. faults that do not extent upward beyond the Rupelian layer) and the *upper fault array* (i.e. faults that detach downwards into the Rupelian layer) (Fig. 4).

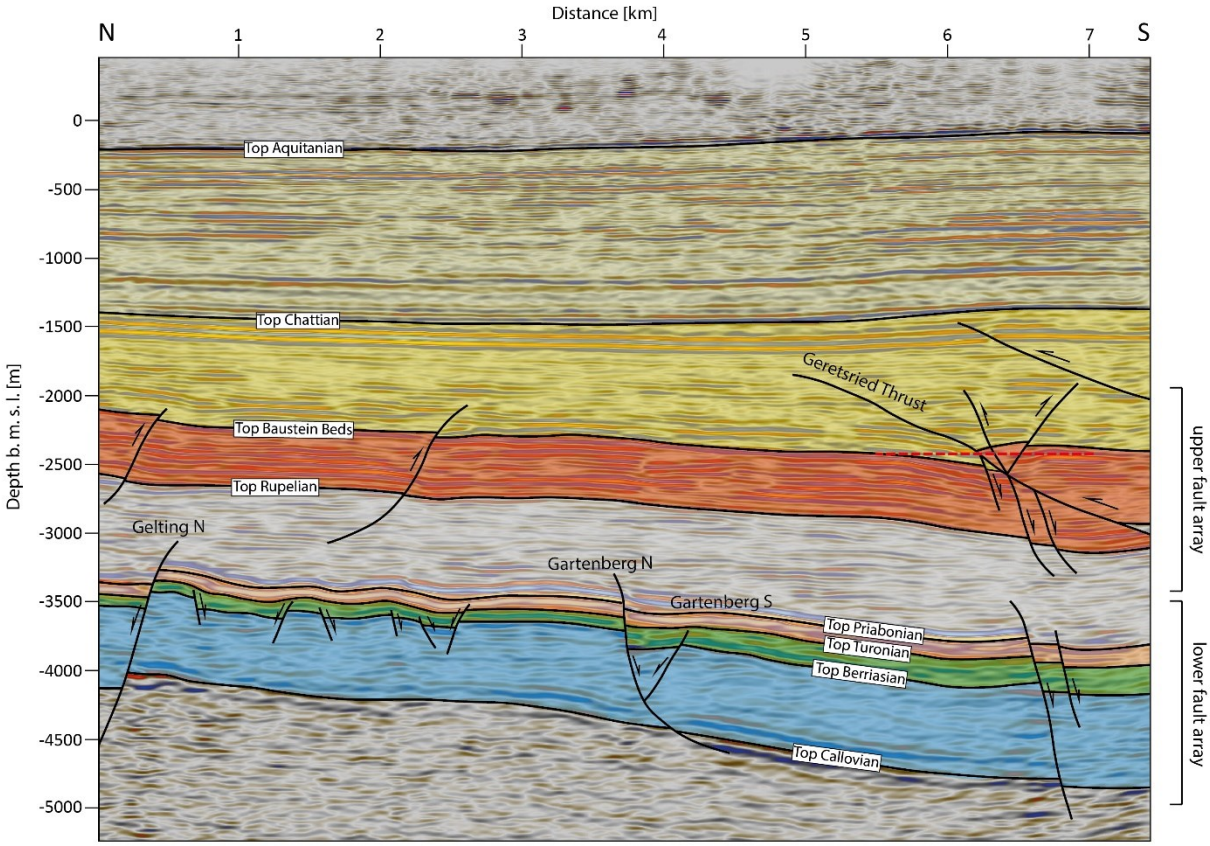

Figure 4: N–S seismic profile through the study area (for location, see Fig. 1). The red dashed line marks the location of the horizontal slice in Figure 3.

3.1. Lower fault array

The lower fault array consists of normal faults that are longitudinal with respect to the Alpine deformation front, striking either ENE –WSW or E–W, and have opposing basinward and forelandward dip directions (Fig. 5). In cross-section, the majority of the faults appear planar and dip 75° to 85°, except for Fault Gartenberg S and Fault Gartenberg N that have shallower dip angles of 60° to 65° (Fig. 4) in the upper section of the reservoir and flatten out in its lower section. In map view, the faults have a subtle corrugated shape (Fig. 5).

With respect to their vertical extent and the stratigraphy they displaced, the lower faults are subdivided, for descriptive purposes, into major and minor faults. The major faults offset crystalline basement and tip-out upward into the Rupelian claystones, whereas the minor faults show no discernible offset of the basement and tip-out upward within either the Turonian or lowermost Rupelian claystones. The fault tips of the minor faults that do not breach the Turonian claystone layer are overlain by monoclines that indicate extensional forced folds.

Major conjugate faults define two prominent graben structures in the NW and centre of the study area. The NW- and N-dipping graben-bounding faults accommodate the largest throws across these structures, with a maximum of c. 180 m at top Callovian on Fault Gelting South and c. 150 m at top Berriasian on Fault Gartenberg South. Displacement along the northern flanks of the grabens is distributed across SE- and S-dipping, conjugate and secondary, antithetic faults.

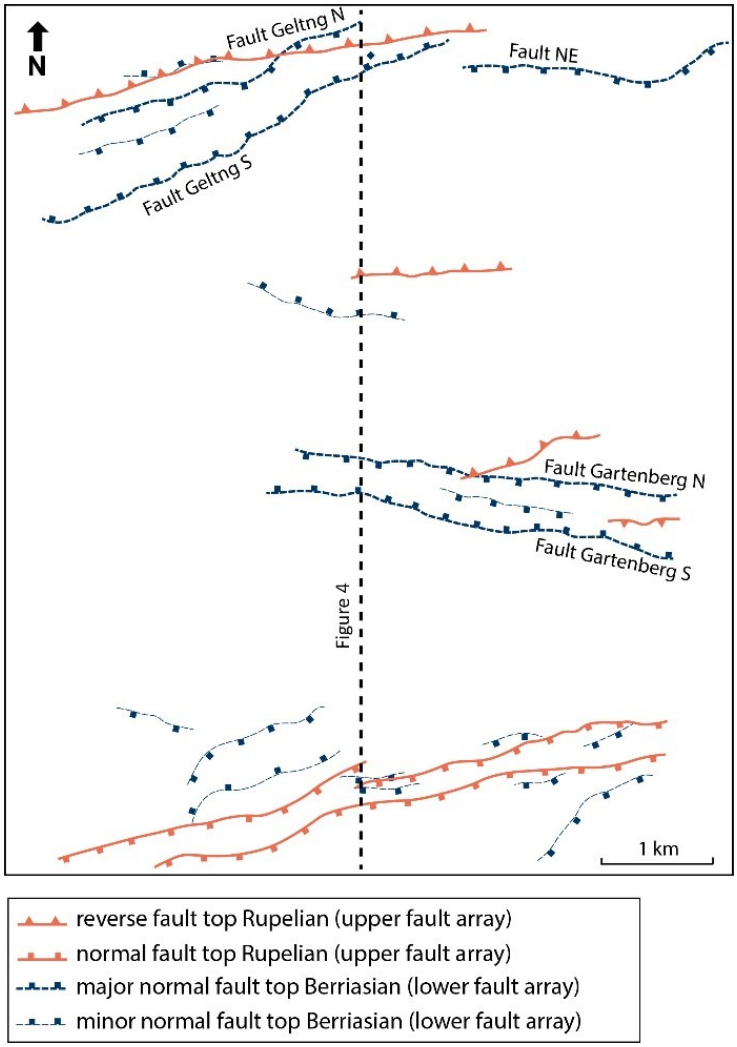

Figure 5: Map of fault traces picked within the 3D seismic volume. Upper faults (orange lines) and lower faults (blue lines) have the same strike direction.

Isopach maps of the Upper Jurassic carbonate platform, Cretaceous, and Priabonian Molasse units reveal no significant intraformational thickness changes across the lower faults, except for the aforementioned thinning of the carbonate platform within the central graben (Fig. 6a, Fig. 6b, Fig. 6c; figures are at the end of the article). In contrast, there is a major thickness increase of the Rupelian claystone sequence within the downthrown blocks of the major lower faults (Fig. 6d; figure is at the end of the article).

Juxtaposition diagrams of four seismic-stratigraphic horizons offset by Fault NE and Fault Gartenberg South are plotted in Figure 7 and Figure 8. In both juxtaposition diagrams, the largest amount of fault throw accrued at top Berriasian, decreasing towards both younger and older strata. The major difference in throw distribution along the selected faults is represented by local throw minima on Fault NE at top Turonian, which is not observed for Fault Gartenberg South.

3.2. Upper fault array

The upper fault array exhibits fault geometries that indicate normal faulting in the southern part of the study area and reverse faulting in its central and northern parts. The upper faults strike approximately in the same direction as the faults below, showing some lateral offset with respect to their lower counterparts. Much like the lower faults, the upper faults have alternating dip directions; dipping either to the S or to the N (Fig. 5). The dip angles of the reverse faults range from 50° to 60°, whereas the normal faults dip steeper (65°-70°). In the south, the major low-angle Geretsried Thrust overprints the normal faults. In the cross-section, it has a prominent stepover within a linkage zone, i.e. relay ramp, between two of the normal faults (Fig. 4). The hanging-wall of the Geretsried Thrust is extensively deformed by folding and back-thrusting. Directly above the Geretsried Thrust, the Neogene sediments are tilted and dip northwards(Fig. 4).

The upper faults offset mechanically competent Baustein Beds and die out upward into the Chattian Sands and downward into the Rupelian claystones. Most probably, the faults flatten out within the soft Rupelian claystones and are listric in shape. However, this could not be recognised in the seismic data with certainty due to the almost transparent character of the reflections within the Rupelian interval.

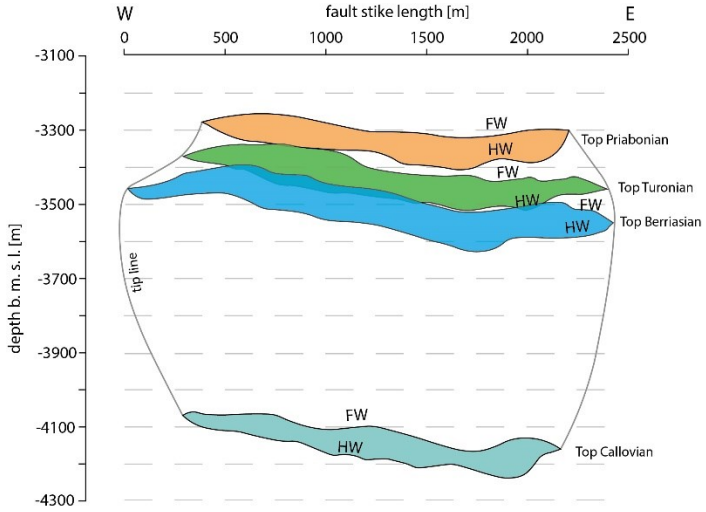

Figure 7: Juxtaposition diagram for Fault NE.

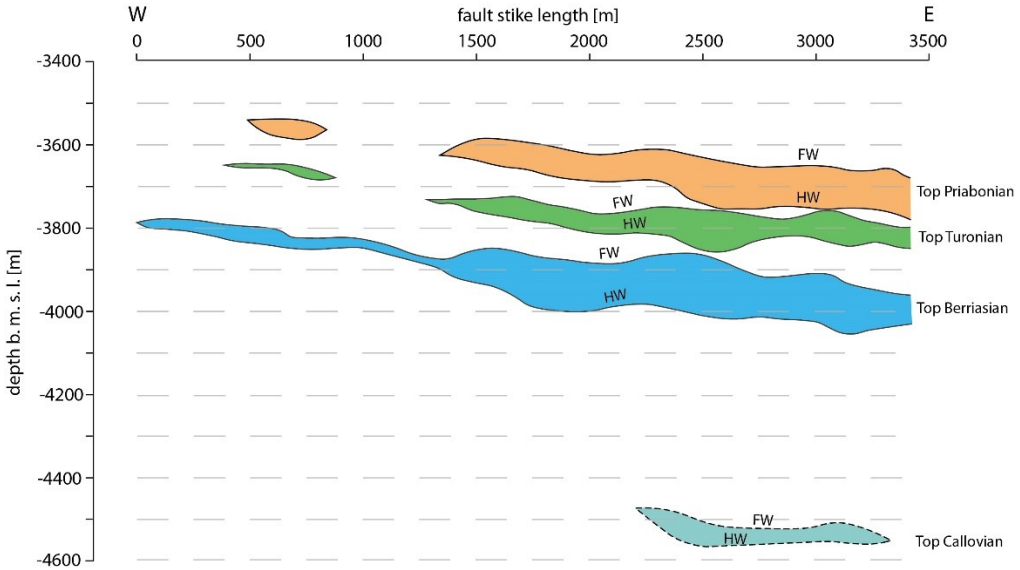

Figure 8: Juxtaposition diagram for Fault Gartenberg South.

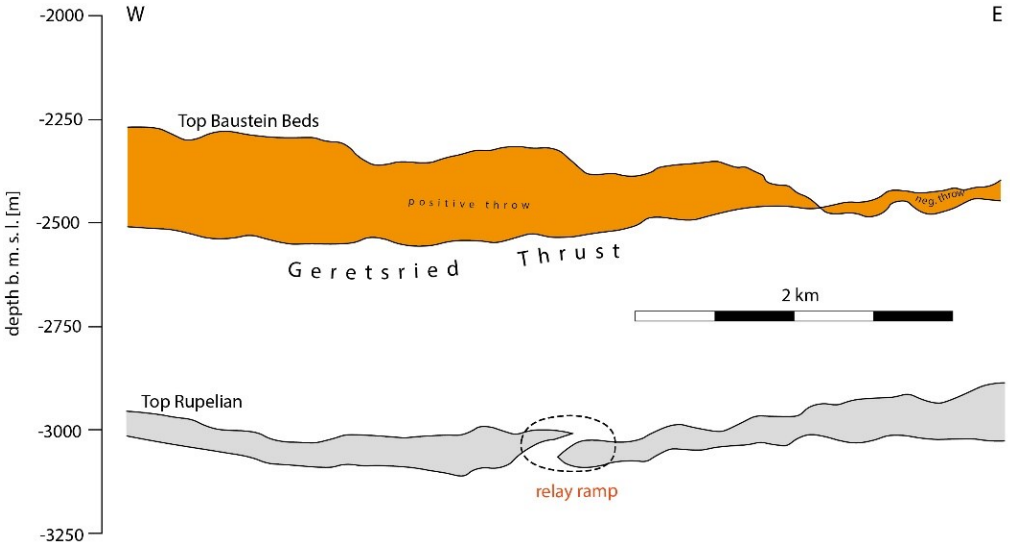

Figure 9: Juxtaposition diagram for the Geretsried Thrust at Top Baustein Beds (orange) and two soft-linked normal faults below at Top Rupelian (grey). Note the eastward decrease of fault throw along the Geretsried Thrust.

The reverse faults have subtle throw magnitudes that do not exceed 50 m at both top Rupelian and top Baustein Beds. In contrast, the normal faults reach maximum throw values at top Rupelian that are twice as much as the reverse faults (Fig. 9). The vertical displacement along the Geretsried Thrust has the maximum of c. 250 m in the westernmost part of the study area. It rapidly decreases to the east, reaching negative throw values because the normal fault offset below is not completely reversed. The hanging-wall anticline of the Geretsried thrust flattens out also in the eastward direction (Fig. 10; figure is at the end of the article).

4. DISCUSSION

4.1 Structural analysis

Lower fault array

The fault throw analysis of the major lower faults reveals that the maximum throw accumulated at the top of the carbonate platform and decreases both down-dip and up-dip (Fig. 7, Fig. 8). From this observation, we suggest that the fault initiated within the carbonate platform and grew by radial propagation towards the younger and older strata. However, substantial fault throw at near top crystalline basement (top Callovian) suggests that the basement was already pre-faulted at a previous tectonic stage, since it is unlikely that the downward propagation of the studied faults could offset intact, rigid, crystalline rock. We therefore hypothesise that the pre-existing basement structures attracted later extensional deformation, whereby the point of maximum displacement migrated along the slip plane away from the point of fault reactivation within the basement, upward into the carbonate interval. A possible explanation for this scenario is fault development by vertical segment linkage in the presence of a mechanical barrier (e.g. Childs et al., 1996; Wilkins and Gross, 2002). During reactivation, propagation of the pre-existing basement faults was restricted within the mechanically incompetent clays and fine sandstones of the Dogger. As a result of the restriction, a new fault segment formed within brittle carbonates above and, as the slip continued, eventually connected with the basement fault segment below. We assume that the displacement minima at top Callovian represents the location of the fault linkage. In contrast, the minor faults that do not offset top Callovian, must have developed within the carbonate platform as individual faults without interaction with basement precursor faults.

To assess the timing of faulting of the lower fault array, we use the seismic-stratigraphic observations from seismic sections, juxtaposition diagrams, and isochore maps. The seismic section in Figure 4 clearly shows that the Rupelian sediments blanket the upper tips of the lower faults. Furthermore, there are indications of growth strata above the central graben. Thickening of the Rupelian strata across the hanging-walls of the lower faults indicates their syn-kinematic nature (Fig. 6d). These observations suggest that the lower faults were active during the early Rupelian times and their activity ceased before the Rupelian sedimentation was complete. A very likely trigger for the observed extensional faulting is the flexural bending of the foreland plate in response to the northward-advancing Alpine thrusts. Presumably, the zone of maximum flexure reached the study area by the early Rupelian, which facilitated a temporal stress field with negative effective minimum stress oriented perpendicular to the trend of the foredeep (Tavani et al., 2015). As the maximum curvature zone migrated further northwards in later Rupelian times, the fault activity ceased.

We can explain the maximum throws at the top of the carbonate platform (top Berriasian), which are evident from the juxtaposition diagrams, with two fault evolution scenarios; (1) accumulation of cumulative throw at top Berriasian due to the multiphase activity of the lower faults and (2) restriction of fault propagation by mechanical barriers above top Beriassian.

The former scenario implies that the faults were initially active prior to the Rupelian times and were later reactivated during the Rupelian, whereby a cumulative throw accumulated at top Berriasian. Fault initiation must have occurred following the deposition of top Berriasian. Recent studies in the Molasse Basin suggest that the main fault activity occurred during Late Jurassic-Early Cretaceous times (e.g., Moeck et al., 2015; Budach et al., 2017). This is in a good agreement with the regional tectonics at this time; the European passive continental margin experienced thinning due to the opening of the Penninic Ocean to the south. However, this scenario requires indication of growth faulting such as thickness increase of the Cretaceous sediments across the faults, which is not evident from the isochore map (Fig 6c).

On the contrary, we are in favour of the later scenario, in which the lower fault array initiated and died out during the Rupelian, whereby the gradual upward decrease of fault throw from top Berriasian to top Priabonian can be attributed to the effects of mechanical stratigraphy. We propose that the faults initiated within the carbonate platform and radially propagated up-dip until they encountered Turonian claystones. Here, much of the offset was accommodated by monoclinal folding due to ductile deformation of the incompetent layer. The high displacement gradient below the incompetent layer can be attributed to the active thinning and thickening of the Turonian claystones in the damage zone.

Forced extensional folding in a monoclinal style above the upper tips of the minor faults that do not breach the Turonian claystones is indicative of blind fault propagation (Baudon and Cartwright, 2008). The faults failed to interact with the free surface during the Rupelian due to the inhibition of further up-dip propagation through the incompetent claystone layer.

Following the abovementioned considerations, we propose the following kinematic evolution sequence for the lower fault array, based on the example of the major Fault NE (Fig. 11):

1. Pre-existing basement faults attracted extensional deformation within the carbonate platform, whereby individual fault segments initiated and grew within the brittle carbonate platform.
2. Fault segments propagated radially upward, where they were arrested by the multi-layered mechanical stratigraphy, and downward, linking with their basement precursors. Incompetent layers up-dip deform by ductile flow, resulting in folding of the above-lying layers. Growth-strata began to form in the syn-kinematic Rupelian sequence.
3. As fault slip continued, the faults breached the monocline. Eventually, faulting ceased and the stagnant fault tip was buried by the later Rupelian sediments.

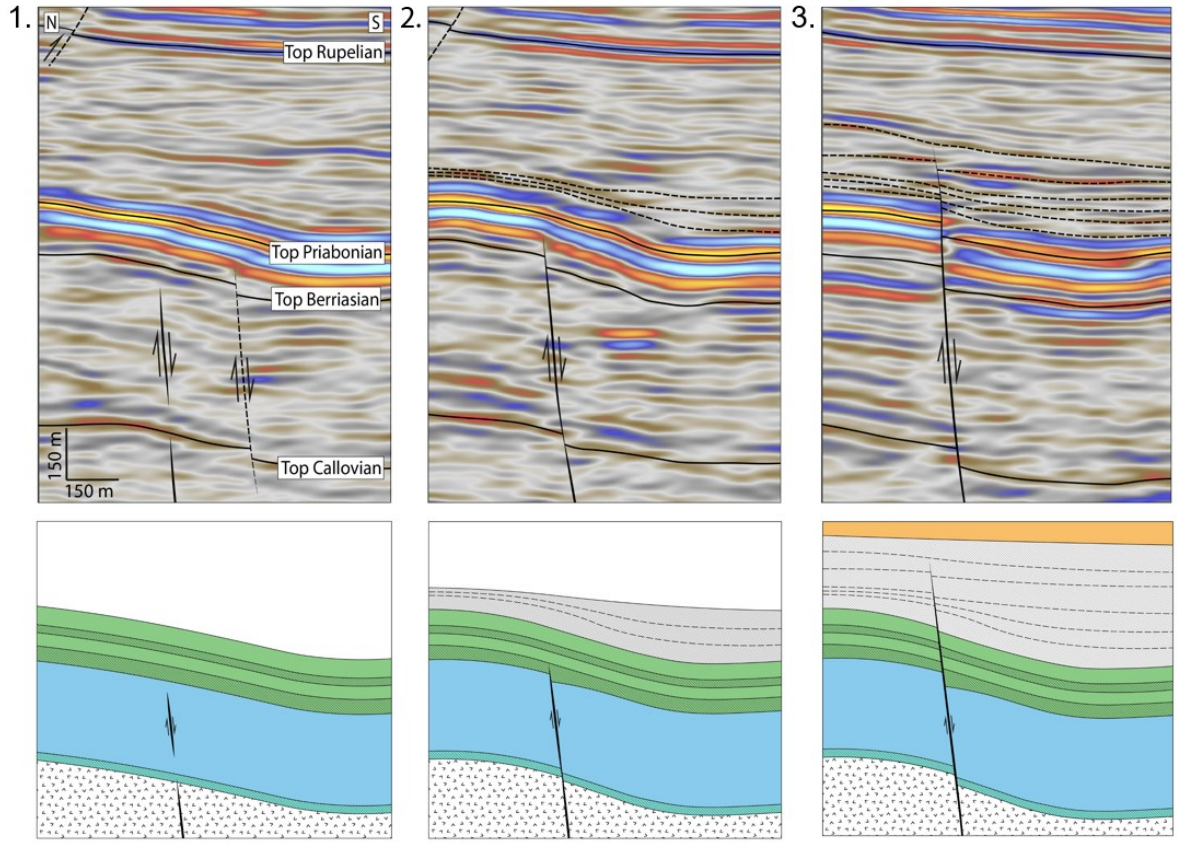

Figure 11: Stages in both temporal and spatial evolution of Fault_NE. For

Upper fault array

The seismic interpretation revealed that the upper fault array experienced both extensional and compressional deformation. The steep dip angles of the reverse faults suggest that they formed initially as normal faults. These normal faults do not extend thought the Chattian Sandstones, whilst the Baustein Beds exhibit uniform thickness distribution without any major thickness changes across the faults. We therefore can imply that the normal faults of the upper fault array formed during the Chattian. We speculated in the previous subchapter that the maximum curvature zone migrated further north from the study area in the late Rupelian. Therefore, the external tectonic stresses are unlikely triggers of the Chattian normal faulting. Instead, we attribute the initiation of normal faults within the competent Baustein Beds to the gravitational sliding or differential compaction that is conditioned by the thick incompetent Rupelian claystones that are in the overpressured state (Drews et al., 2018). Subtle fault throws that we observe on our fault are typical for the differential compaction faults (Bruce, 1973; Xu et al., 2015). The upper normal faults did not connect downward with the lower faults. The former fault most probably flatten out and eventually terminate within the Rupelian claystones.

The contractional deformation succeeded the extensional phase at the study area during mid-Miocene times, as the Alpine thrusts propagated north. The stress regime within the Cenozoic Molasse changed, so that the maximum horizontal stress got oriented perpendicular to the Alpine deformation front. The longitudinal normal faults became preferentially oriented within the active stress field, thus allowing reactivation as reverse faults. The normal faults to the south were too steep to be reactivated as reverse faults. Instead, they became overprinted by a major thrust. The Geretsried Thrust nucleated within the Baustein beds, where they had been weakened by pre-existing normal faults.

4.2 Implications for geothermal exploration and targeting

Fault networks within the Upper Jurassic carbonate platform are the prime drilling targets for geothermal exploration in the Molasse Basin. Several geothermal projects successfully extract geothermal heat from major fault zones in the reservoir rock (e.g. Unterhaching geothermal site; Lüschen et al., 2011). However, there are also cases when drilling into a major fault zone resulted in low production rates due to low permeability of a fault (Mauerstetten Fault; Mraz et al., 2017). This clearly shows that drilling into a fault zone delineated with the help of seismic data does not necessarily guarantee successful geothermal production. The “Foreland basin” play type reveals complex deformation patterns that range from extensional to compressional faults and show both decoupled (thin-skinned) and coupled (thick-skinned) deformation style. Therefore, depending on the kinematic history of the faults and their orientation within the present-day stress field, faults possess varying hydraulic conductivity within the deep geothermal reservoir. In the following paragraph, we discuss the hydraulic potential of the lower fault array based on the results of the structural analysis.

Reinecker et al. (2010) suggest that the Molasse basin is most likely under a strike-slip to thrust faulting regime with the maximum horizontal stress in approximately N-S direction. The results of our structural analysis confirm the thrust faulting regime for the Cenozoic fill of the Molasse Basin, which implies high magnitudes of maximum horizontal stress also within the carbonate reservoir. In the present-day stress field, the ENE–WSW or E–W normal faults of the lower fault array are perpendicularly oriented to the maximum horizontal stress direction and therefore, irrespective of the fault regime at the reservoir level, have low slip potential.

Moreover, the high normal stresses acting on the fault planes exclude any dilational potential for the investigated faults; instead, contraction on the E–W faults is presumed. Furthermore, the results of the fault throw analysis revealed that the lower faults were most likely inactive since Rupelian times. The prolonged inactivity of the faults could have a negative impact on their transmissivity; dormant faults are more likely to be healed by secondary mineralization. These observations suggest that the lower faults are likely to act as barriers to fluid flow. However, the hydraulic tests of the well Geretsried GEN-1ST-A1 indicate open fractures in a tight reservoir (Fig. 12). In total, mud losses of more than 800 m^3 were recorded during drilling. The elevated permeability could be explained by the intersection of secondary antithetic faults within the rollover anticline in the hangingwall of Fault Gartenberg S. These secondary faults must have formed to accommodate strain associated with hangingwall folding as the listric fault was developing. We infer that the hangingwall folding facilitated the development of an extensive network of interconnected fractures that remained permeable despite high normal stresses.

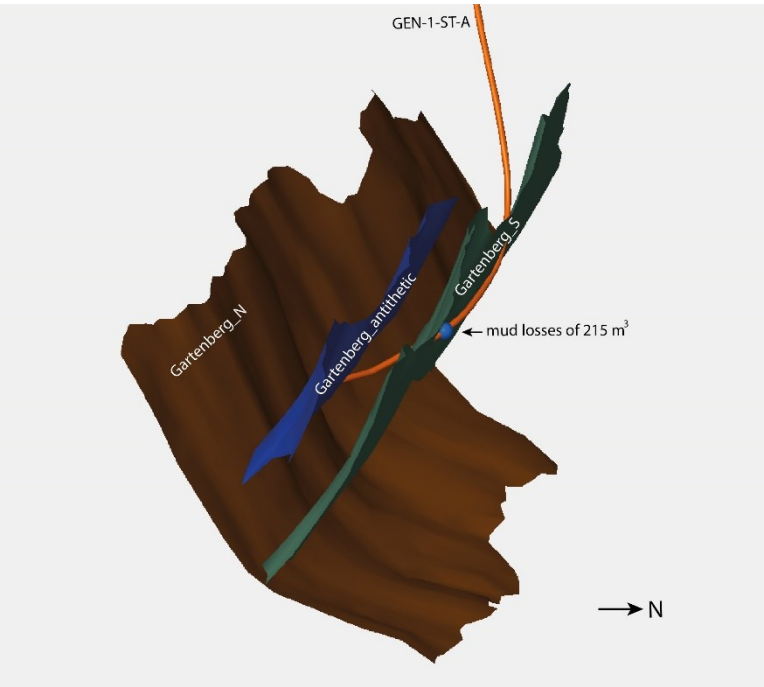

Figure 12: Model of the central (Gartenberg) graben showing location of the high mud losses in the sidetrack well GEN-1-ST-A

5. CONCLUSIONS

The present study shows that the various strata at Wolfratshausen have undergone different deformation phases; extension in the pre- and/or early-orogenic stages of basin formation and contraction in Miocene times. The Cenozoic extension includes two intermittent faulting events: one in the Rupelian and one in the Chattian. The southern part of the German Molasse Basin is characterized by decoupled deformation, separated by the thick Rupelian claystone sequence. In our work, we show that the mechanical stratigraphy governs the deformation style in the Molasse Basin.

The identified structures and deformation style indicate an active stress regime and thus provide insight into the hydraulic transmissivity of the fault zones. Results of the seismic interpretation and kinematic analysis show that the Upper Jurassic carbonate reservoir of the Wolfratshausen prospect is controlled by isolated, longitudinal normal faults. The occurrence of contractional deformation in the Tertiary Molasse indicates presently high horizontal stresses in this region, combined with high vertical stresses at depth. We therefore postulate that the faults in the Mesozoic strata exhibit reduced hydraulic connectivity due to high normal stresses resolved on the fault plane. Only fault intersection zones, as areas of increased fracture density, may be hydraulically connected, as suggested by mud loss in the geothermal well Geretsried GEN-1ST-A1.

By this work, we emphasize the importance of detailed structural analysis for reservoir characterization of deep geothermal aquifers in the Molasse Basin as well as other foreland basins worldwide according to the geothermal play type concept. We show that seismic interpretation should cover the entire stratigraphic pile and not only focus on the reservoir itself. Such strategy should be adopted for the pre-drilling stage of the future geothermal exploration in the Molasse Basin to increase drilling success rates.

REFERENCES

Allan, U. S.: Model for hydrocarbon migration and entrapment within faulted structures, AAPG Bull, **73**, (1989), 803–811.

Allen, P.A., Crampton, S.L., Sinclair, H.D.: The inception and early evolution of the North Alpine Foreland Basin, Switzerland. Basin Res., **3**, (1991), 143-163.

Anderson, T.R. and Fairley, J.P: Relating permeability to the structural setting of a fault-controlled hydrothermal system in southeast Oregon, USA. Journal of Geophys. Res., **113**, (2008), B05402, doi:10.1029/2007JB004962.

Bachmann, G. H., G. Dohr, and M. Müller: Exploration in a classic thrust belt and its foreland, Bavarian Alps, Germany, AAPG Bulletin, **66**(12), (1982), 2529–2542.

Bachmann, G. H., M. Müller, and K. Weggen: Evolution of the Molasse basin (Germany, Switzerland), Tectonophysics, **137**, (1987), 77–92.

Bachmann, G. H. and M. Müller: Sedimentary and structural evolution of the German Molasse Basin, Eclogae Geologicae Helvetiae, **85**, (1992), 519–530.

Baudon, C., Cartwright, J.A.: 3D seismic characterisation of an array of blind normal faults in the Levant Basin, Eastern Mediterranean. Journal of Structural Geology, **30**(6), (2008), 746–760.

Bruce, C.H.: Pressured shale and related sediment deformation: mechanism for development of regional contemporaneous faults. American Association of Petroleum Geologists Bulletin, **57**(5), (1973), 878–886.

Budach, I., I. Moeck, E. Lüschen, and M. Wolfgramm: Temporal evolution of fault systems in the Upper Jurassic of the Central German Molasse Basin: case study Unterhaching, Int J Earth Sci (Geol Rundsch), **107**, (2017), 635–654.

Childs, C., Nicol, A., Walsh, J.J., Watterson, J.: Growth of vertically segmented normal faults. Journal of Structural Geology **18**(12), (1996), 1389–1397.

Diem, B.: Die Untere Meeresmolasse zwischen Saane (Westschweiz) und der Ammer (Oberbayern): Ecl. Geol. Helv., **79**, (1986), p. 493–559.

Drews, M. C., Bauer, W., Caracciolo, L., Stollhofen H.: Disequilibrium compaction overpressure in shales of the Bavarian Foreland Molasse Basin: Results and geographical distribution from velocity-based analyses. Marine and Petroleum Geology, **24**; (2018), 929–924.

Eisbacher, G.: Molasse – Alpine and Columbian: Geoscience Canada, **1**, (1974), 47–50.

Ferrill D. A., Morris A. P., McGinnis R.N.: Crossing conjugate normal faults in field exposures and seismic data. AAPG Bull, **93**(11), (2009), 1471–1488

Frish, W.: Tectonic progradation and plate tectonic evolution of the Alps: Tectonophysics, **69**, (1979), 121-139.

Lemcke, K.: Zur nachpermischen Geschichte des nördlichen Alpenvorlandes: Geologica Bavarica **69**, (1973), 5-48.

Lemcke, K.: Geologie von Bayern; I, Das bayerische Alpenvorland vor der Eiszeit: Stuttgart, E. Schweizerbart'sche Verlagsbuchhandlung, (1988), 175 p.

Lüschen, E., M. Dussel, R. Thomas, and R. Schulz: 3D seismic survey for geothermal exploration at Unterhaching, Munich, Germany, First Break, **29**(1), (2011), 45–54.

Marfurt, K. J: Techniques and best practices in multiattribute display. Interpretation, **3,** (2015), B1–B23.

Meyer, R. K. F., and H. Schmidt-Kaler: Paläogeographischer Atlas des Süddeutschen Oberjura (Malm), Geol. Jahrb., Reihe A: Allg. und Reg. Geol. BR Dtschl. und Nachbargebiete, **115**, (1990), 77 p., Fed. Inst. for Geosci. and Nat. Resour., Hannover, Germany.

Moeck, I.: Catalog of geothermal play types based on geologic controls, Renewable and Sustainable Energy Reviews, **37**, (2014), 867-882.

Moeck, I., Uhlig S, Loske B, Jentsch A, Ferreiro Maehlmann R, Hild S: Fossil multiphase normal faults: prime targets for geothermal drilling in the Bavarian Molasse Basin? *Proceedings*, World Geothermal Congress, Melbourne, Australia, (2015).

Mraz, E., Moeck, I., Bissman, S., Hild, S.: Multiphase fossil normal faults as geothermal exploration targets in the Western Bavarian Molasse Basin: Case study Mauerstetten, Z. Dt. Ges. Geowiss., 169(3), 2018, 389–411.

Müller, M., F. Nieberding, and A. Wanninger: Tectonic style and pressure distribution at the northern margin of the Alps between Lake Constance and the Rivver Inn, Geol. Rundsch., **77**(3), (1988), 787–796.

Ortner, H., S. Aichholzer, M. Zerlauth, R. Pilser, and B. Fügenschuh: Geometry, amount, and sequence of thrusting in the Subalpine Molasse of western Austria and southern Germany, European Alps, Tectonics, **34**, (2015), 1–30.

Pfiffner, O. A.: Tectonic evolution of Europe - Alpine Orogeny. In: Blundell, D., Freeman, R. & Mueller, S. (eds.) A Continent Revealed: The Eropean Geotraverse. Cambridge, U.K.: University Press Cambridge, (1992).

Reinecker, J., M. Tingay, B. Müller, and O. Heidbach: Present-day stress orientation in the Molasse Basin, Tectonophysics, **482**, (2010), 129–138.

Schulz, R., R. Thomas, R. Jung, and R. Schellschmidt: Geoscientific prospect evaluation for the Unterhaching geothermal power plant, Z. Angew. Geol., **50**(2), (2004), 28–36.

Sheridan, J.M. and Hickman, S.H: In situ stress, fracture, and fl uid fl ow analysis in well 38C-9: An enhanced geothermal system in the Coso geothermal field. *Proceedings,* 29th Workshop on Geothermal Reservoir Engineering, Stanford University, Stanford, CA, Jan 26-28, (2004).

Sissingh, W.: Tectonostratigraphy of the North Alpine Foreland Basin: correlation of Tertiary depositional cycles and orogenic phases: Tectonophysics, **282**, (1997), p. 223-256.

Tavani, S., F. Storti, O. Lacombe, A. Corradetti, J. A. Muñoze, and S. Mazzoli: A review of deformation pattern templates in foreland basin systems and fold-and-thrust belts: Implications for the state of stress in the frontal regions of thrust wedges, Earth-Science Reviews, **141**, (2015), 82–104.

von Hagke, C., Lujiendjik, E., Ondrak, R., Lindow, J.: Quantifying erosion rates in the Molasse basin using a high resolution data set and a new thermal model. Geotect. Res. **97**, (2012), 94–97.

von Hartmann H., D. C. Tanner, and S. Schumacher: Initiation and development of normal faults within the German alpine foreland basin: The inconspicuous role of basement structures, AGU Tectonics, **35**, (2016), 1560–1574.

Weides, S., and J. Majorowicz: Implications of spatial variability in heat flow for geothermal resource evaluation in large foreland basins: the case of the Western Canada Sedimentary Basin, Energies, **7**(4), (2014), 2573–2594.

Wilkins, S.J., Gross, M.R.: Normal fault growth in layered rocks at Split Mountain, Utah: influence of mechanical stratigraphy on dip linkage, fault restriction and fault scaling. Journal of Structural Geology; **24**(9), (2002), 1413–1429.

Xu, S., Hao, F., Xu, C., Wang, Y., Zou, H., Gong, C.: Differential compaction faults and their implications for fluid expulsion in the northern Bozhong Subbasin, Bohai Bay Basin, China. Marine and Petroleum Geology, **63**, (2015), 1–16.

Ziegler, P. A.: Geological Atlas of Western and Central Europe: The Hague, Shell Internationale Petroleum Maatschappij, B.V., (1990), 239 p.

Ziegler, P. A., Cloetingh, S. & van Wees, J.-D: Dynamics of intra-plate compressional deformation: the Alpine foreland and other examples. Tectonophysics, **252**, (1995), 7–59.

Zweigel, J., 1998, Eustatic versus tectonic control on foreland basin fill. Sequence stratigraphy, subsidence analysis, stratigraphic modelling, and reservoir modelling applied to the German Molasse Basin: Contr. Sedimen. Geol, Stuttgart, E. Schweizerbart'sche Verlagsbuchhandlung, **20**, (1998), 140 p.

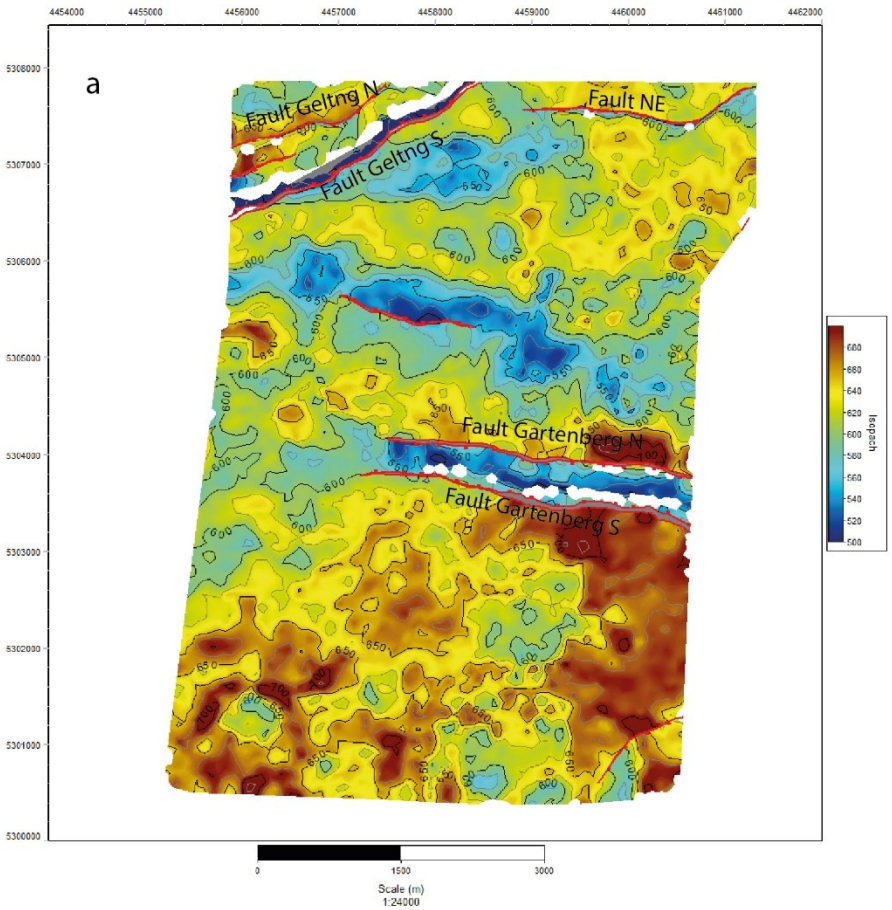

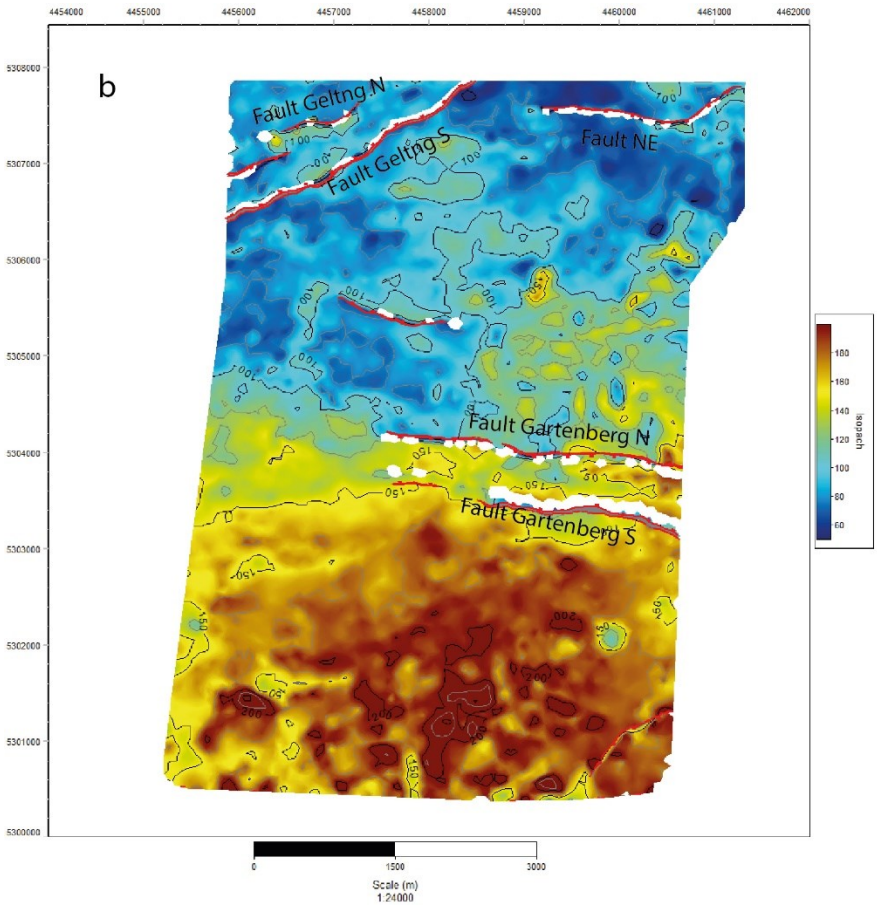
b
Fault Geltng N
Fault Geltng S
Fault NE
Fault Gartenberg N
Fault Gartenberg S
Isopach
Scale (m)
1:24000

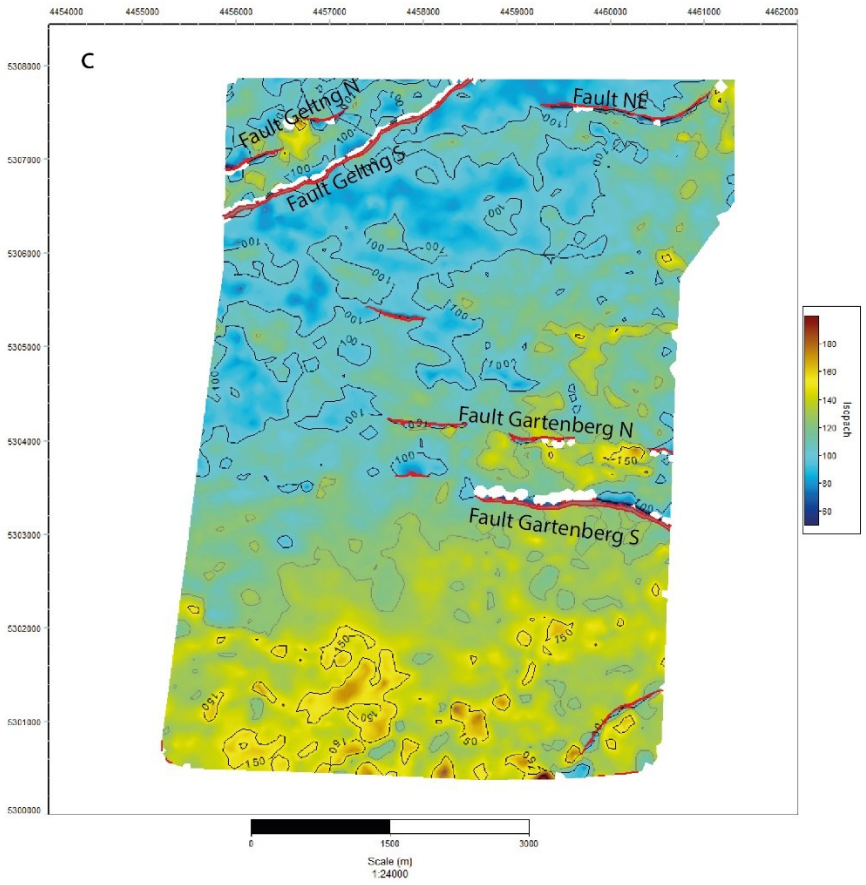
c
Fault Geltng N
Fault Geltng S
Fault NE
Fault Gartenberg N
Fault Gartenberg S
Isopach
Scale (m)
1:24000

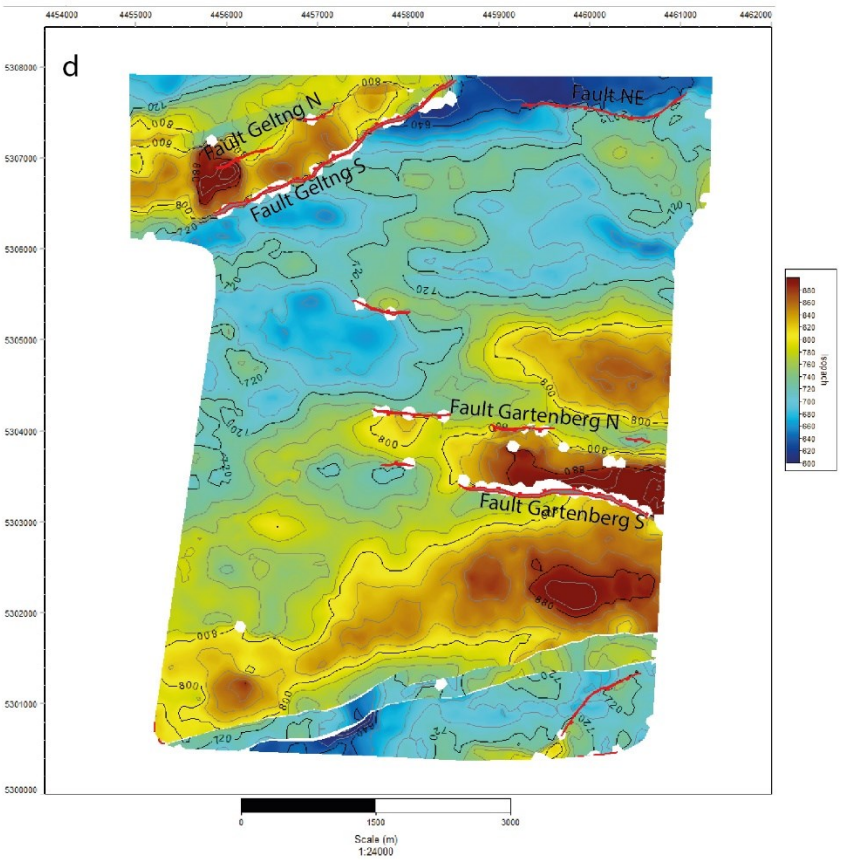

Figure 6: Isochore maps for the intervals (a) Upper Jurassic carbonate platform, (b) Cretaceous unit, (c) Priabonian Molasse unit, and (d) Rupelian unit.

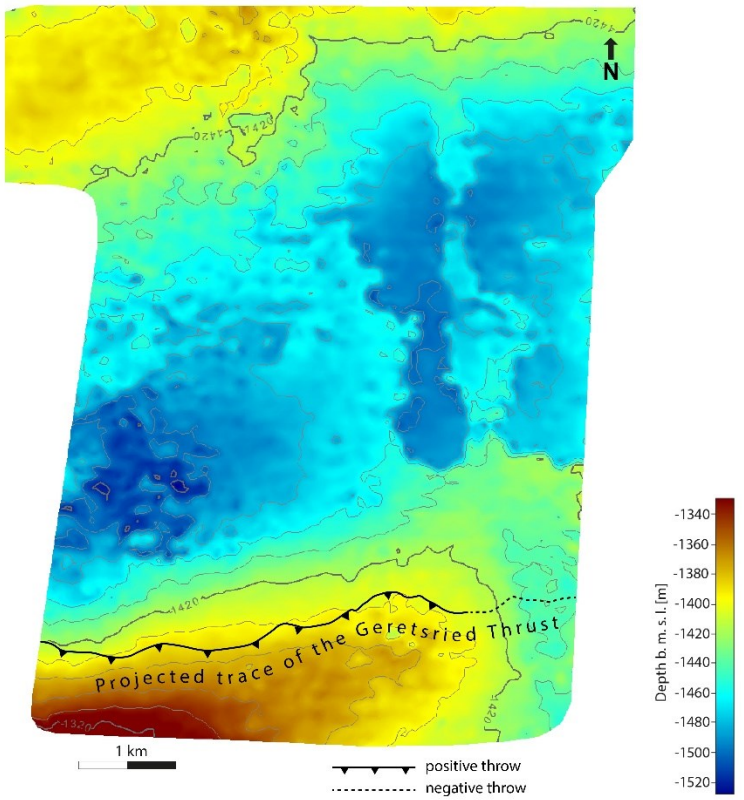

Figure 10: Depth map of Top Chattian. Note eastward termination of the anticlinal structure (fault-related fold) as the Geretsried Thrust dies out.